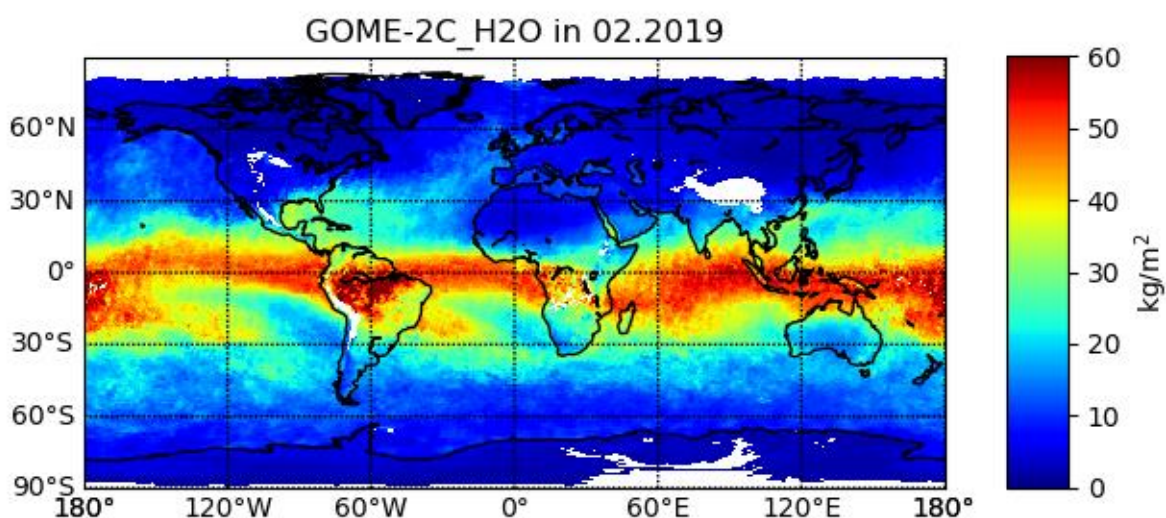


AC SAF VALIDATION REPORT

Validated product:

Identifier	Name	Acronym
O3M-386	Off-line Total H ₂ O from GOME-2C	MCG-O-H2O



Authors:

Institute

Name

Sander Slijkhuis

Niilo Kalakoski

German Aerospace Center

Finnish Meteorological Institute

Document Change Record

Document, Version	Date	Changes	Originator
1.0	2020.03.30	Original version	S. Slijkhuis, N. Kalakoski

Table of Contents

1	Introduction	4
1.1	Purpose.....	4
1.2	Definitions, acronyms and abbreviations	4
1.3	Applicable documents	5
1.4	Structure of the report	5
2	Intercomparison GOME-2C and GOME-2B	6
2.1	GOME-2 total column water vapour product.....	6
2.2	Comparison of daily measurements	6
2.3	Comparison of monthly averages	9
2.4	Discussion and conclusion.....	19
2.5	Reference Documents	19
3	Comparison against radiosonde and GPS observation.....	20
3.1	Introduction	20
3.2	Reference observations and co-locations.....	20
3.3	Results.....	23
3.4	Reference Documents.....	29

1 Introduction

1.1 Purpose

This report presents the results of a verification of the Total Column Water Vapor (TCWV) level 2 product from the ultraviolet spectrometer Global Ozone Monitoring Experiment-2 (GOME-2) on METOP-C, to investigate if the quality of the product is sufficient that operational status may be assigned to the product. The verification has been carried out as comparison to operational data from GOME-2 on METOP-B, and comparison to ground based water vapour observations. The verification has been carried out by the AC SAF. The Level 2 [reprocessed] GOME-2 H₂O column data, generated by DLR using the GOME Data Processor (GDP) version 4.9, are used.

The overall consistency between TCWV measurements from the various GOME-2 instruments is evaluated in the overlap period February 2019 to July 2019.

1.2 Definitions, acronyms and abbreviations

AMF	Air Mass Factor
CM SAF	EUMETSAT Satellite Application Facility on Climate Monitoring
DOAS	Differential Optical Absorption Spectroscopy
EUMETSAT	European Organisation for the Exploitation of Meteorological Satellites
GCOS	Global Climate Observing System
GOME-2	Global Ozone Monitoring Experiment-2
GOME-2A	GOME-2/MetOp-A
GOME-2B	GOME-2/MetOp-B
H ₂ O	Water Vapour
HOAPS	Hamburg Ocean-Atmosphere Parameters and Fluxes from Satellite
METOP	Meteorological Operational Satellite
O3MSAF	EUMETSAT Satellite Application Facility for Atmospheric Composition and UV radiation
REMSS	Remote Sensing System
RMS	Root Mean Square Error
SSM/I	Special Sensor Microwave/Imager
SSMIS	Special Sensor Microwave Imager Sounder
TCWV	Total Column Water Vapor
UPAS	Universal Processor for UV/VIS Atmospheric Spectrometers
VCD	Vertical Column Density

1.3 Applicable documents

- [AD-1] **ATBD** Algorithm Theoretical Basis Document for GOME-2 Total Column Products of Ozone, NO₂, SO₂, BrO, H₂O, HCHO and Cloud Properties, DLR/GOME-2/ATBD/01, Rev. 3/A, P. Valks et al., October 2016.
- [AD-2] **PUM** Product User Manual for GOME-2 Total Columns of Ozone, NO₂, SO₂, BrO, H₂O, HCHO, and Cloud Properties, DLR/GOME-2/PUM/01, Rev. 3/A, Valks, et. al., October, 2016.
- [AD-3] **ATBD** Algorithm Theoretical Basis Document for GOME-2 NO₂ and H₂O Level 3 Climate Products, SAF/O3M/DLR/ATBD/Clim, M. Grossi, et al., 2016.
- [AD-4] **ATBD** Algorithm Theoretical Basis Document HOAPS (2011) release 3.2 Ref Number: SAF/CM/DWD/ATBD/HOAPS. Andersson et al., 2011
- [AD-5] **PRD** O3M SAF Product Requirements Document, SAF/O3M/FMI/RQ/PRD/001/Rev. 1.7, J. Hovila, et. al., 2015

1.4 Structure of the report

The structure of this report is as follows.

Section 2 presents an intercomparison of the H₂O columns retrieved from GOME-2C and GOME-2B. Comparisons of both daily as well as monthly mean measurements are discussed. In Section 3, the validation of the GOME-2C H₂O columns with ground-based measurements are presented. We show the results of the comparisons of GOME-2C H₂O columns against water vapour observations based on radiosoundings from Integrated Global Radio-sonde Archive (IGRA) and GPS observations from Suominet network.

2 Intercomparison GOME-2C and GOME-2B

2.1 GOME-2 total column water vapour product

The GOME-2 total column water vapour product is derived from measurements of the GOME-2 instruments aboard EUMETSAT polar-orbiting MetOp-A, B and C satellites. The GOME-2 instrument is a downward-looking spectrometer operating in the UV/VIS/near-IR wavelength region. GOME-2C and GOME-2B are operated with a swath width of 1920 km and a ground pixel size of 40 x 80 km², whereas GOME-2A is currently operated with a swath width of 960 km and a ground pixel size of 40x40 km. Each of the GOME-2 instruments has a slightly different equator cross time (orbit location offset).

The algorithm used for the retrieval of the H₂O vertical column is based on the classical DOAS method (Wagner et al., 2011) and does not include explicit modeling of the atmospheric radiative transfer [AD-1, AD-2]. Slant columns of H₂O and O₂ are derived from the differential absorption structure in the spectral range between 614 and 683nm. After the DOAS fit, slant columns are corrected for saturation using model results from line-by-line calculations. The conversion from slant columns to vertical columns is performed applying the air mass factor of O₂, in conjunction with an AMF correction factor which accounts for different height profiles of H₂O and O₂. The algorithm deliberately uses a minimum of external input, in order to generate a data set, which is truly independent from global climate models and from other instruments. In the latest version of the retrieval algorithm (Grossi et al., 2015), a further enhancement in the quality of the H₂O total column is introduced by optimizing the cloud screening and developing an empirical correction in order to eliminate the instrument scan angle dependencies. The correction is based on the GOME-2A full time series and is computed separately over land and ocean surfaces, to take into account the diverse reflectivity properties of the surface.

In contrast to other satellite data sets, the GOME-2 product has the advantage that it covers the entire Earth, including both ocean and continents, leading to a more consistent picture of the global distribution of the atmospheric humidity. Moreover, the retrieval is performed in the visible/near-infrared spectral range and it is very sensitive to water vapour in the lower troposphere, which contributes the major fraction of the total atmospheric column.

2.2 Comparison of daily measurements

In this report, the AC-SAF Level 2 product from the “new” GOME-2C instrument is evaluated against the Level 2 product of GOME-2B. Co-location is performed by gridding GOME-2 data on a regular 0.5°x0.5° longitude/latitude grid. An area weighted tessellation procedure is used to bin the product. This is done similar to the generation of the GOME-2 monthly mean TCWV Level 3 product of the AC SAF (product identifier O3M-88). Detailed information about the Level 2 retrieval method for GOME-2 and the aggregation and gridding procedure used to produce the Level 3 monthly products can be found in the AC-SAF SAF ATBD [AD-3].

The dataset covers the period from February 2019 to July 2019. Besides the water vapour product, support data relative to the clouds and surface properties are included in the data set.

Figure 2.1 shows the global distribution of GOME-2C and GOME-2B gridded TCWV data for July 1, 2019. No TCWV has been calculated in the GOME level-2 product for “heavily clouded” pixels. Heavily clouded means here: (cloud fraction) x (cloud albedo) > 0.6 or O₂ column >80% obscured (see ATBD). The TCWV distributions from both instruments look similar. Note that there is a shift in longitude (and measurements time) between the two instruments. Primarily, pixels in the west side of the swath of GOME-2C overlap with pixels in the east side of the swath of GOME-2B. This gives rise to the overlap pattern in the bottom panel of Fig. 2.1, which plots the difference in TCWV between both instruments.

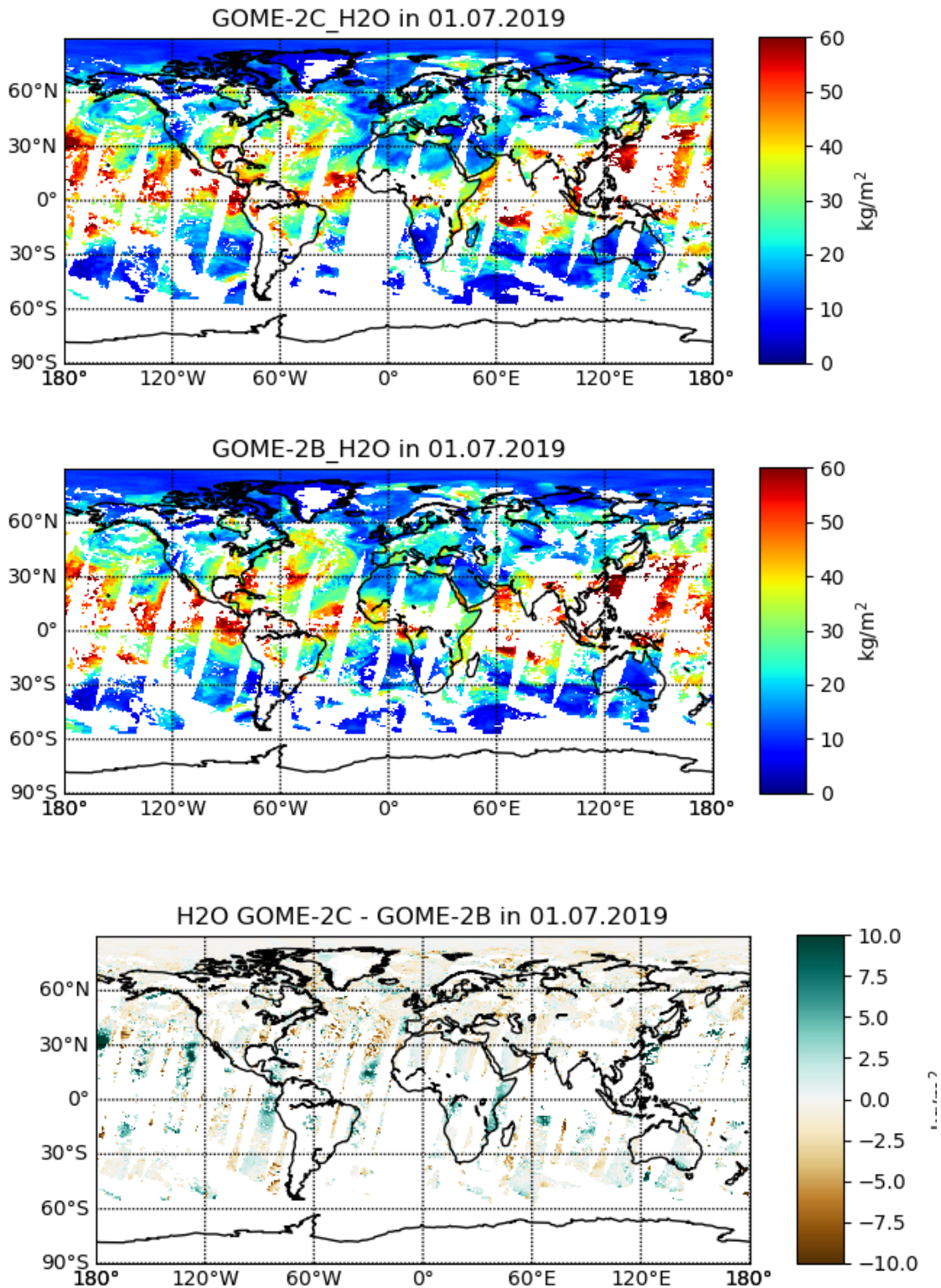


Figure 2-1 Gridded map of TCWV measurements of GOME-2 on July 1, 2019. Top panel: GOME-2C instrument; centre panel: GOME-2B instrument ; bottom: difference (GOME-2C - GOME-2B)

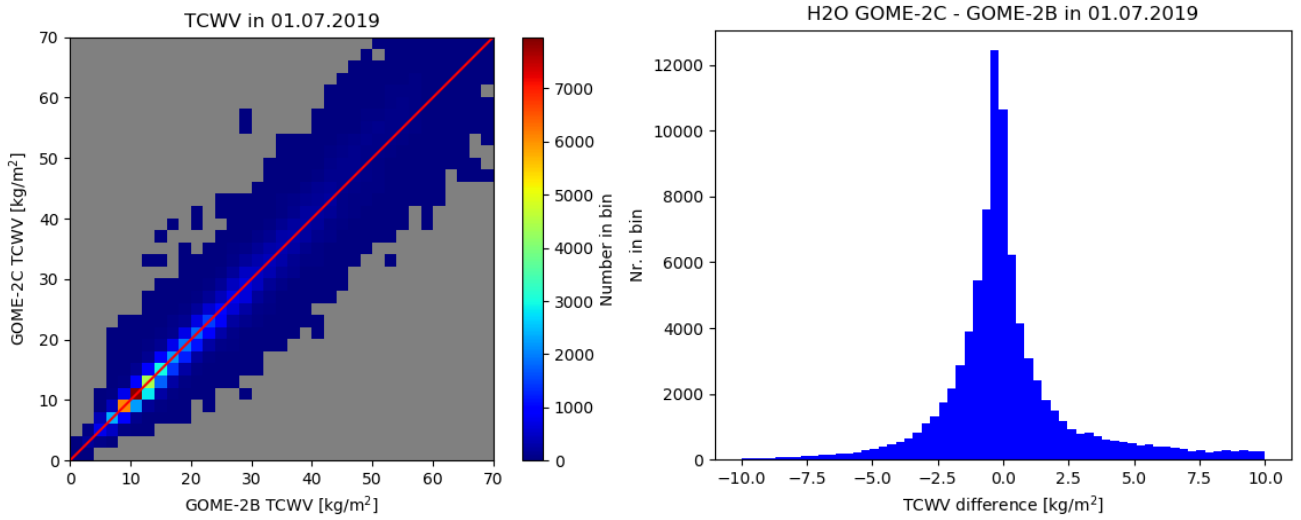


Figure 2-2 Left panel: gridded TCWV measurements of GOME-2C on July 1, 2019 versus those of GOME-2B; right panel: histogram of TCWV difference GOME-2C minus GOME-2B

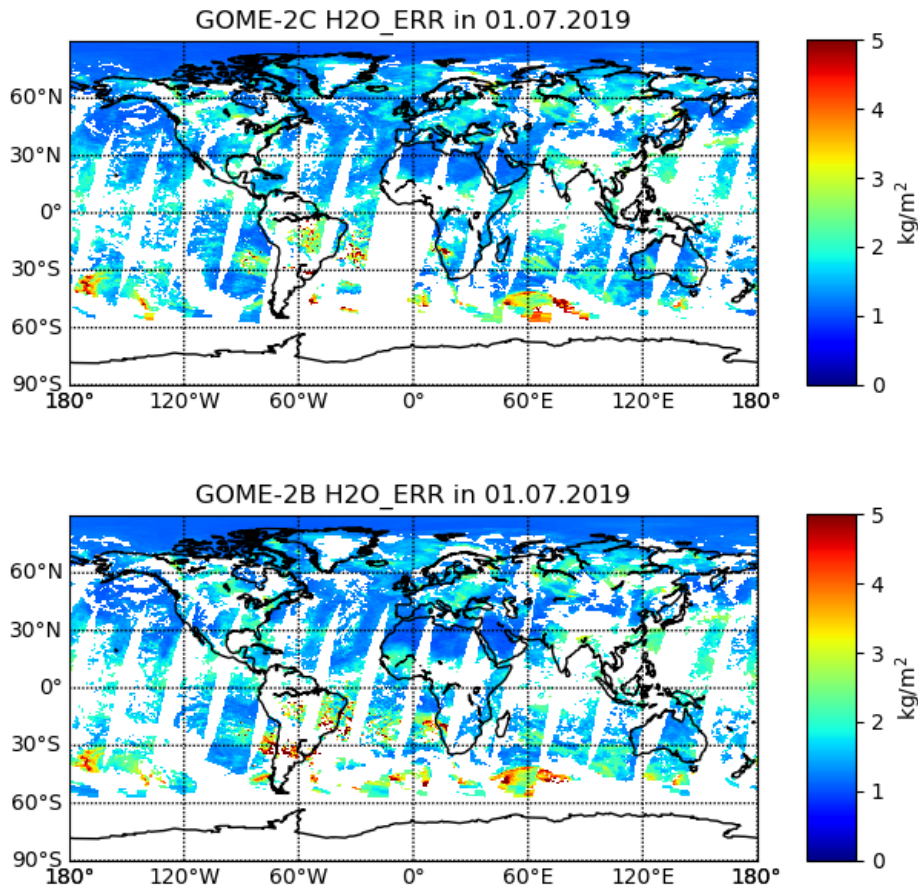


Figure 2-3 Gridded map of TCWV measurement errors of GOME-2 on July 1, 2019. Top panel: GOME-2C instrument; bottom panel: GOME-2B instrument

A scatterplot of the GOME-2C TCWV [kg/m^2] gridded measurements versus GOME-2B TCWV is shown in Figure 2-2 (left panel). The right panel of the figure shows the histogram distribution of the difference in TCWV (GOME-2C - GOME-2B) in each map grid cell.

The average errors on the GOME-2 TCWV product are shown in Figure 2-3; these are very similar for GOME-2C and GOME-2B.

The width of the distribution of the difference (2C - 2B) in the right panel of Figure 2-2 is roughly in line with the TCWV errors from the level 2 products. The tail of the histogram distribution is likely caused by pixels with a considerable fraction of clouds, although the air mass calculation should in principle correct for that. The tail is more or less in line with what has been found in various validation efforts for the GOME-2A and GOME-2B TCWV products, and does not point to any anomaly in GOME-2C.

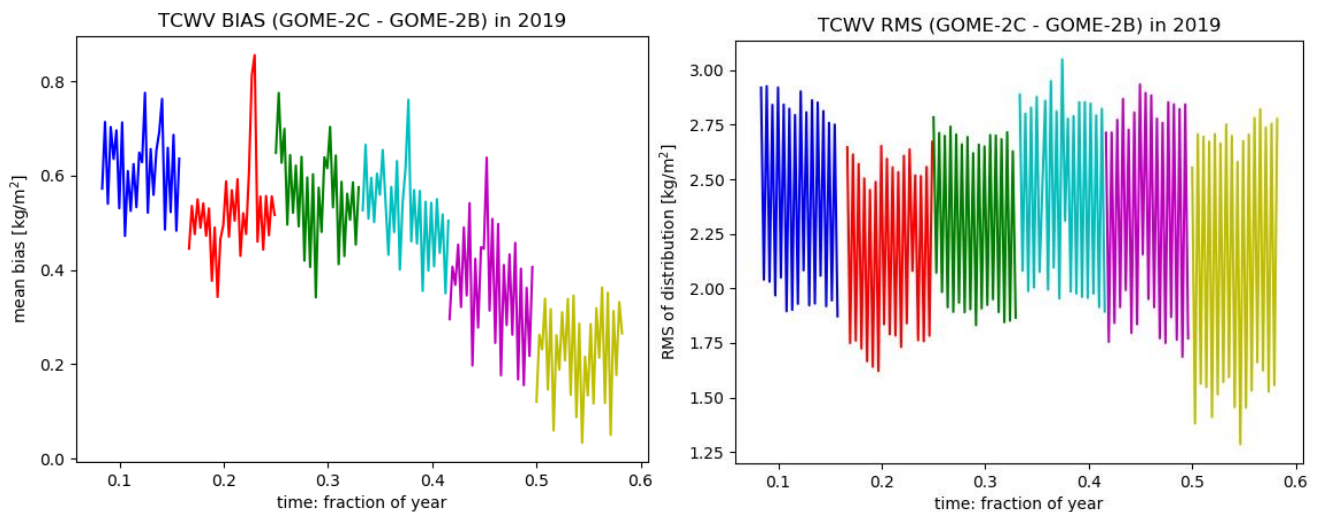


Figure 2-4 Mean bias (left panel) and RMS of the distribution (right panel) of the difference in daily gridded TCWV (GOME-2C - GOME-2B), for each day in the reporting period.

The information in the histogram of Figure 2-2 may be condensed by looking only at the mean bias and the RMS of the distribution in daily TCWV difference. This is depicted for each day of the reporting period in Figure 2-4 (the X-axis labelling denotes time, or days, from February 2019 to July 2019). The figure shows that the mean bias is higher for winter/spring than for the summer days. Especially for the width of the distribution there is a conspicuous alternating day effect.

A discussion of the results is deferred to after the presentation of monthly averaged maps, which have a higher statistical significance per grid cell.

2.3 Comparison of monthly averages

Monthly averages of the gridded TCWV maps from GOME-2C and GOME-2B, and difference in TCWV from (GOME-2C - GOME-2B), is shown in Figures 2-5 and 2-7 for the months February 2019 and July 2019, respectively (these figures are the equivalent of Fig. 2-1, but for monthly average instead of daily measurements). In figures 2-6 and 2-8 the corresponding standard deviation (variability in the daily measurements per grid cell), the number of observations for GOME-2C (per grid cell), and the sum of number of observations of GOME-2C and GOME-2B are shown.

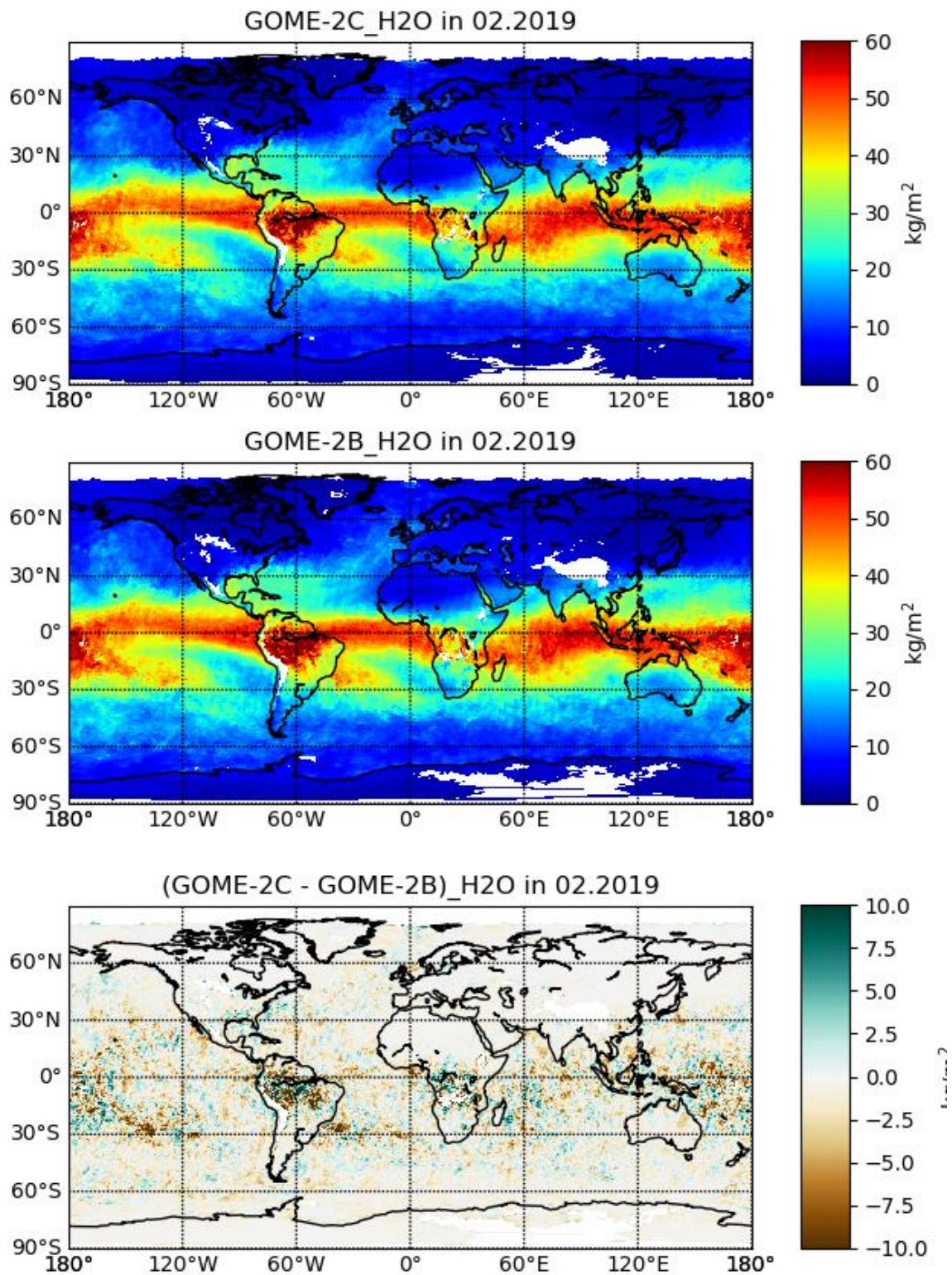


Figure 2-5 Monthly mean TCWV of GOME-2 in February 2019. Top panel: GOME-2C instrument; centre panel: GOME-2B instrument ; bottom: difference (GOME-2C - GOME-2B)

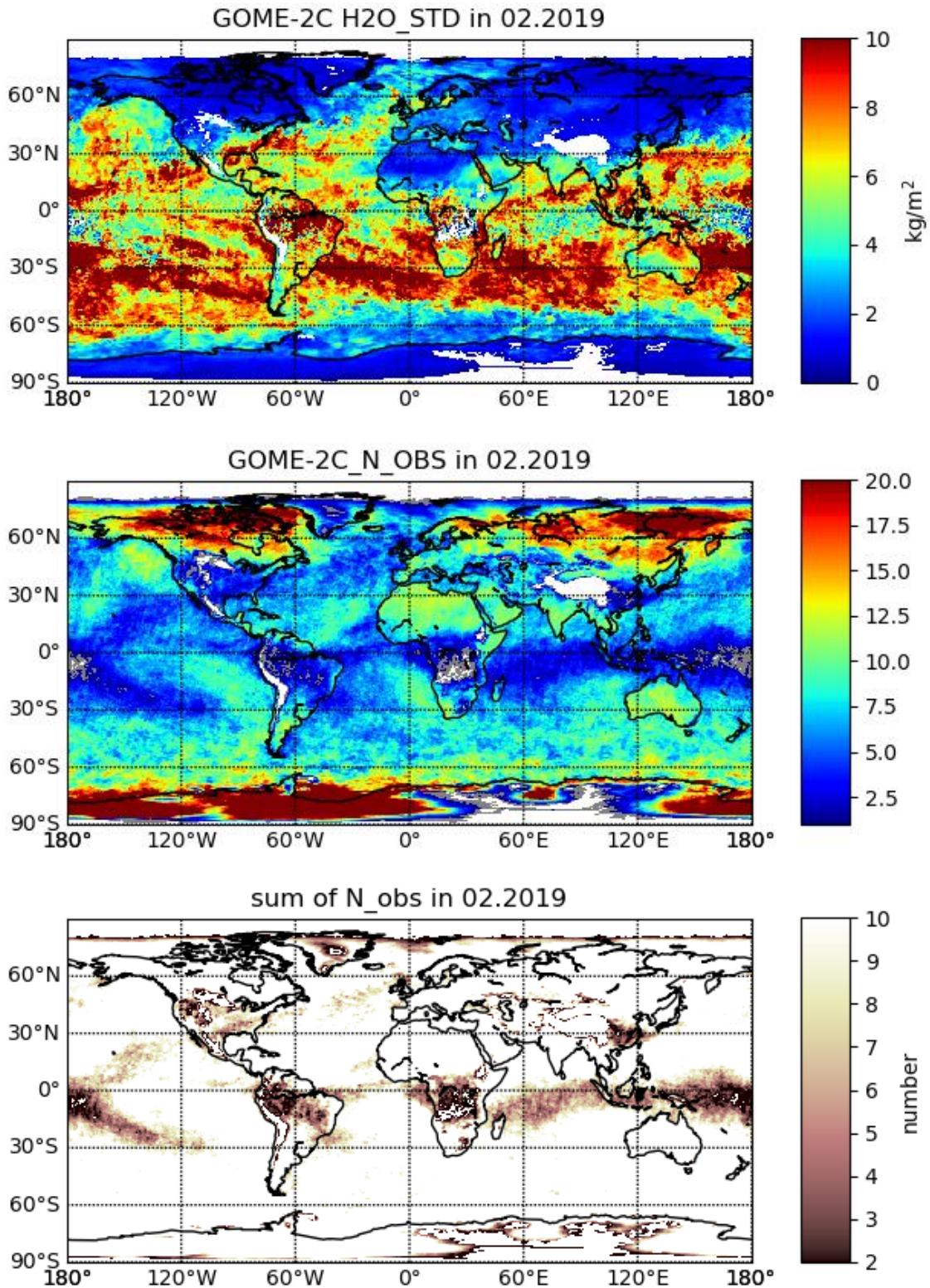
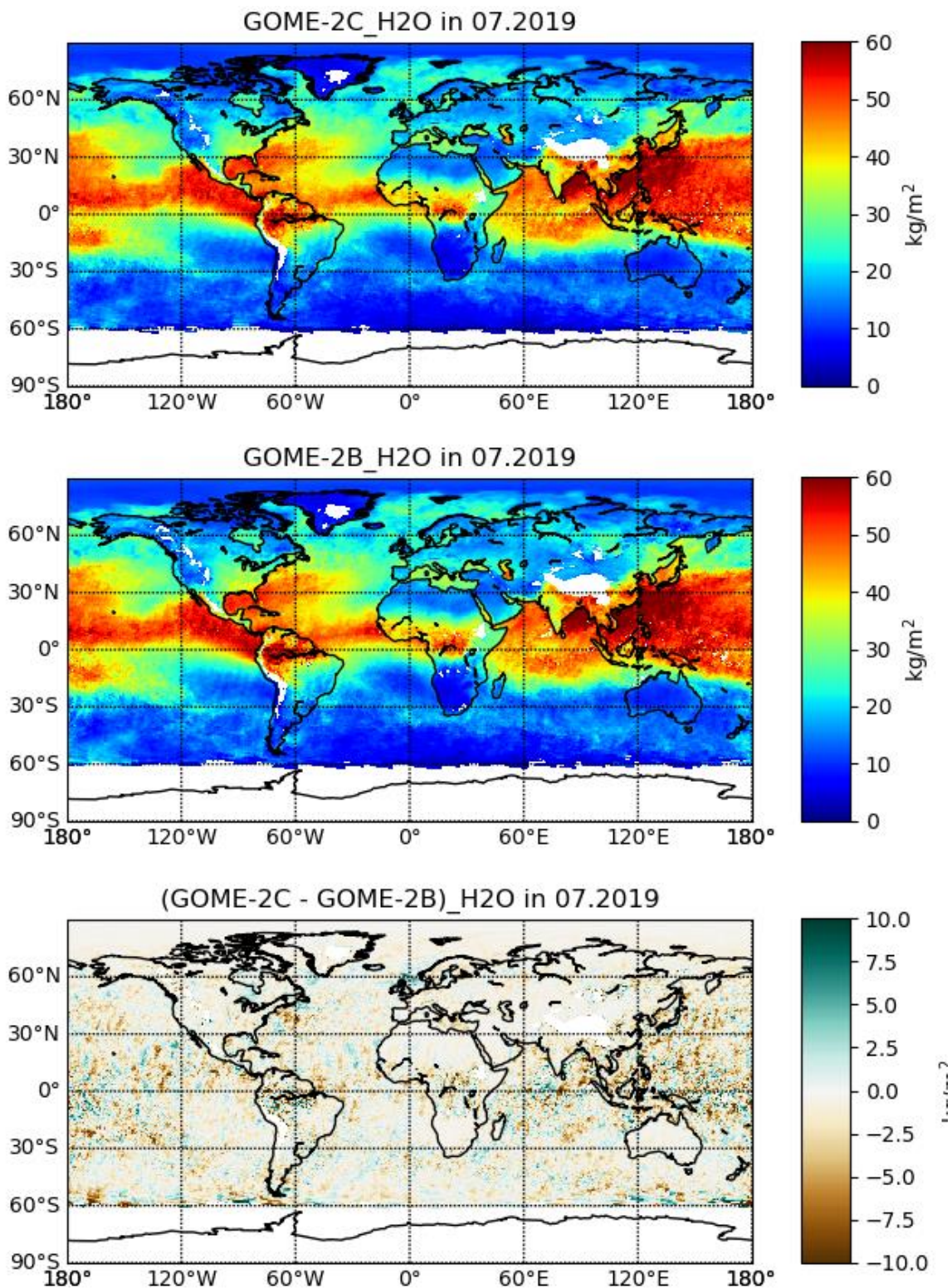


Figure 2-6 Monthly mean data of GOME-2 in February 2019. Top panel: GOME-2C TCWV standard deviation; centre panel: GOME-2C number of observations per grid cell ; bottom: sum of number of observations of GOME-2C and GOME-2B per grid cell.



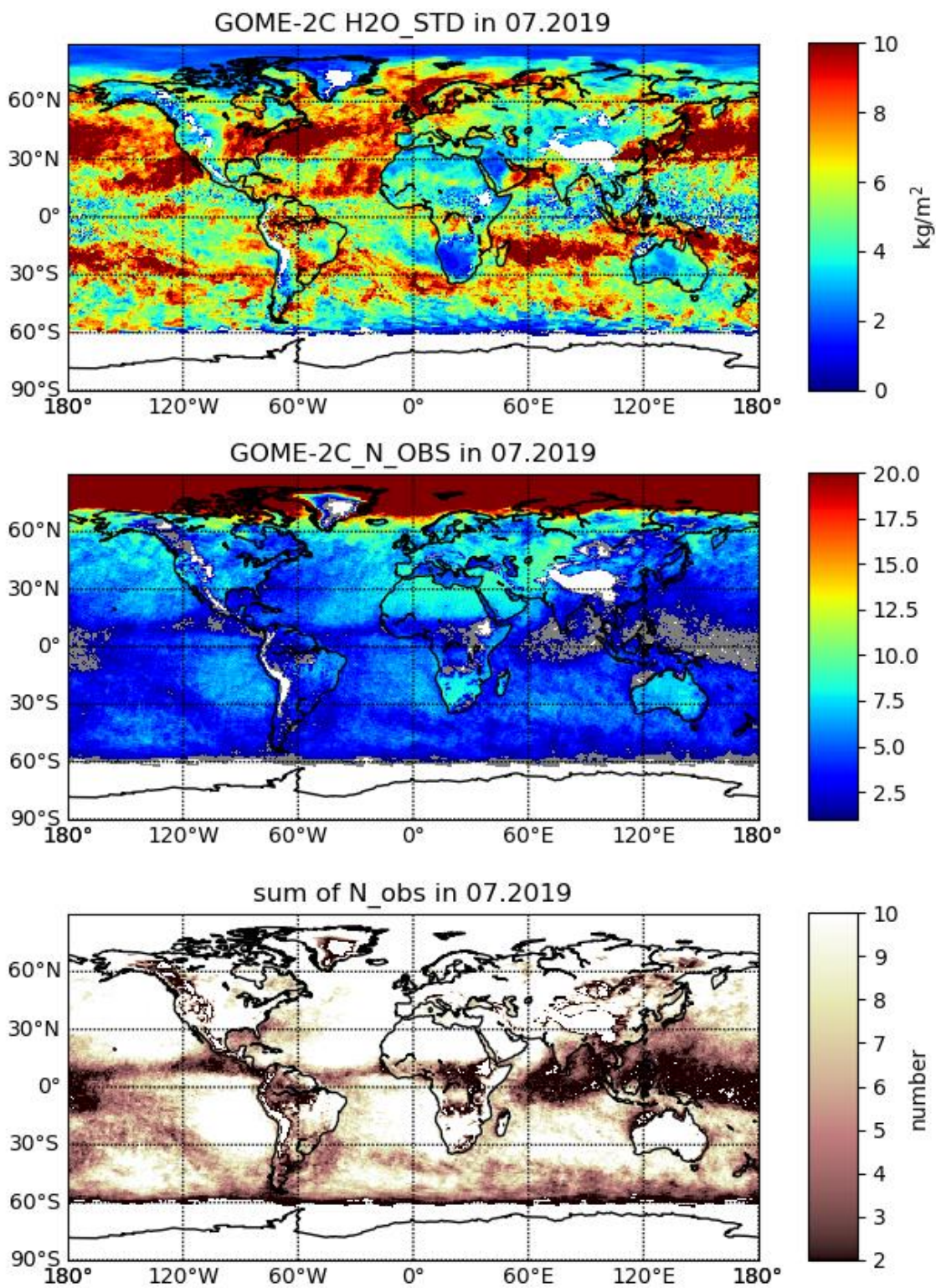


Figure 2-8 As Figure 2-6, but for July 2019.

The maps with number of observations show that the cloud screening is severe in a band around the equator. At mid-latitudes in summer we have statistically the highest cloud fractions (based on earlier GOME-2 validation reports with long time series of GOME-2A TCWV and cloud), but still a sufficient number of observations remain after cloud screening.

The maps of the difference in TCWV between GOME-2C and GOME-2B suggest a minor wet bias for GOME-2C. There is some scatter with higher TCWV differences, but nothing systematic. The higher TCWV differences seem to correlate with a low number of observations; and to some extent with an elevated standard deviation. Such a pattern is not unexpected.

A quantitative comparison between GOME-2C and GOME-2B is shown via the histograms in Figure 2-9, for the months February and July 2019. The bias and RMS of the histograms is shown, for all months, in Figure 2-10. For reasons that will become clear below, we separate between land and sea surface. The histograms are based on the $0.5^\circ \times 0.5^\circ$ grid cells, without a weighting with the number of observations per cell.

The agreement between GOME-2C and GOME-2B is very good, with a mean wet bias of around 0.5 kg/m^2 for GOME-2C w.r.t. GOME-2B, and a RMS difference of around 2 kg/m^2 . There is no significant difference between land and sea surfaces, although the RMS is a bit larger for sea surface in summer.

Remarkable though, is that in the comparison of the level 2 products (*Figure 2-4*) GOME-2C had a dry bias, not a wet bias. Since in the level 2 co-locations pixels in the west side of the swath of GOME-2C coincide with pixels in the east side of the GOME-2B swath, the question is raised if there might be an East-West effect in either instrument.

East-West effects

Maps of monthly averaged gridded TCWV from “East” pixels (the first half of the GOME-2 forward scan) minus monthly averaged gridded TCWV from “West” pixels (the last half of the GOME-2 forward scan) are shown in *Figure 2-11* and in *Figure 2-12*, for the months February and July, respectively. The East-West effect is strikingly similar for GOME-2C and GOME-2B.

While on a regional scale there can be large East-West biases, their distribution looks patchy and without obvious systematics; except that there does seem to be some correlation of large biases with the TCWV standard deviations shown in *Figure 2-6* and *Figure 2-8*.

Histograms of the distribution for GOME-2B are shown in *Figure 2-13* and **Error! Reference source not found.***Figure 2-14*. For GOME-2C the histograms are very similar. For all months the bias, RMS, and skew (3^{rd} moment) of the distribution are plotted in *Figure 2-15*. The East-West bias is about -1.5 kg/m^2 (West higher) for both instruments, for land and sea surface. The width of the distribution is notably larger for sea surfaces, with $\sim 5 \text{ kg/m}^2$, whereas land surfaces have 4.5 in February tapering off to -3.4 kg/m^2 in July. The distributions have a tail to high West biases, as indicated by the skew parameter. There is a pronounced asymmetry towards higher TCWV in West pixels, especially over land surfaces.

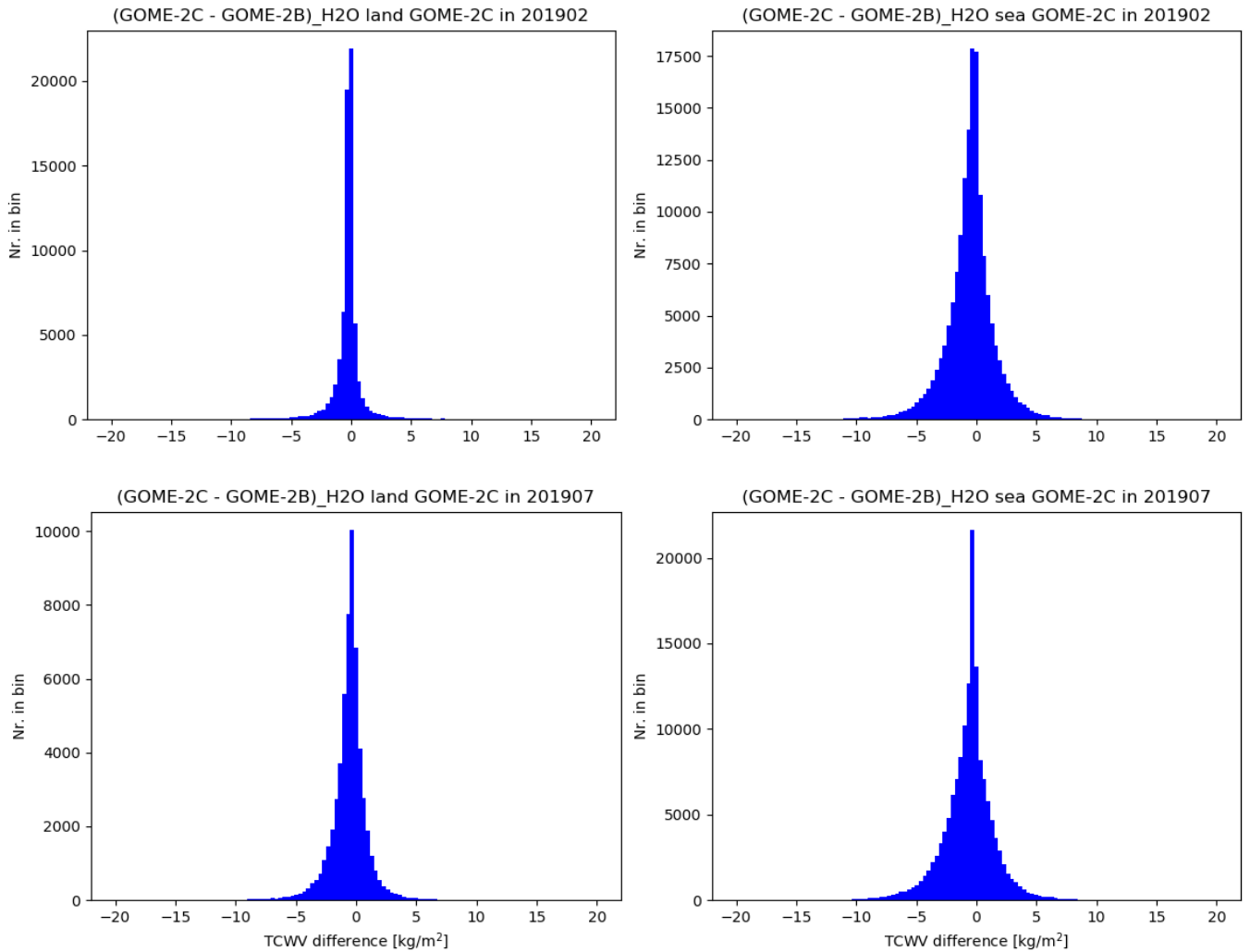


Figure 2-9 Histograms of TCWV difference GOME-2C minus GOME-2B. Top panels: for February 2019. Bottom panels: for July 2019. Left panels are for land surfaces and right panels for sea surfaces.

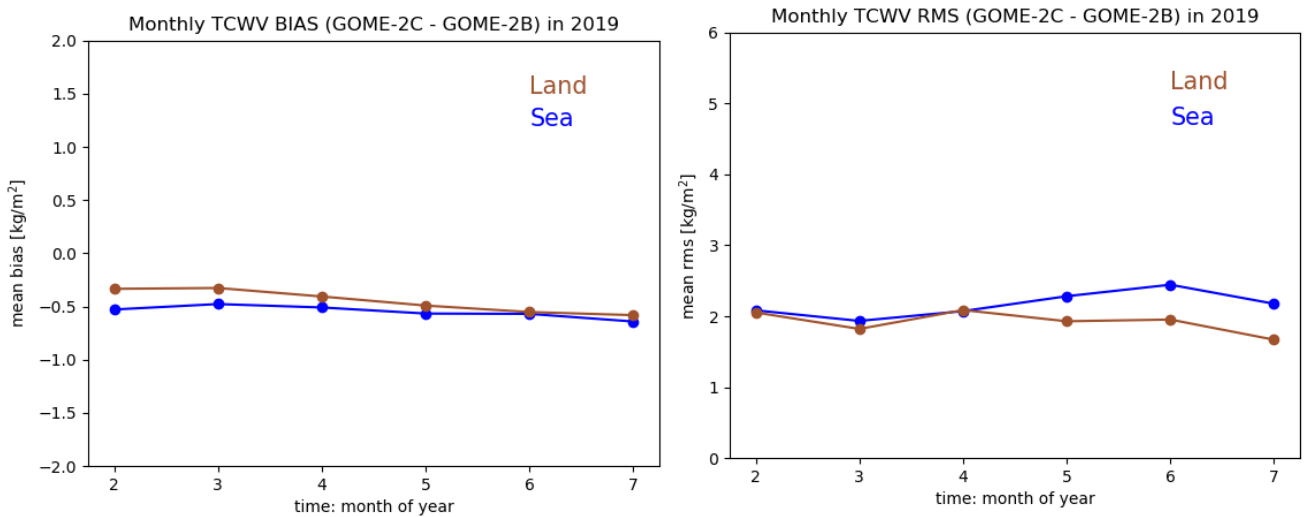


Figure 2-10 Mean bias (left panel) and RMS of the distribution of TCWV difference GOME-2C minus GOME-2B (land brown, sea blue curves)

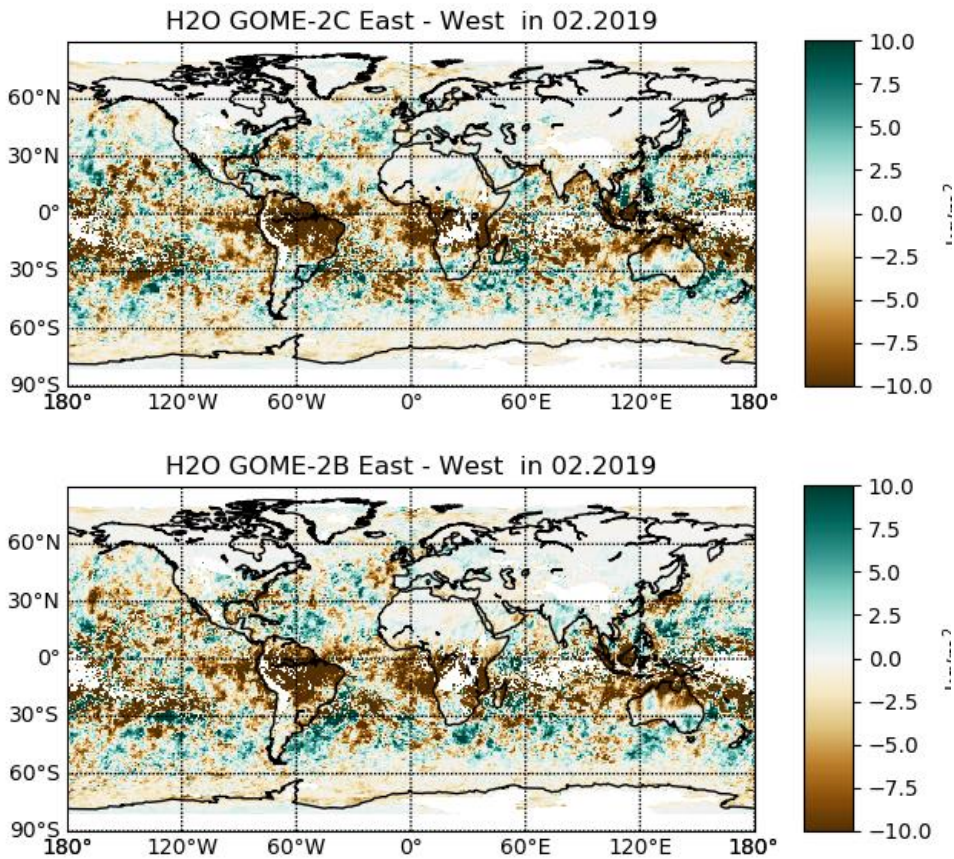


Figure 2-11 Map of monthly averaged gridded TCWV from “East” pixels minus the same from “West” pixels. Top: GOME-2C in Feb.2019; bottom: GOME-2B in Feb.2019.

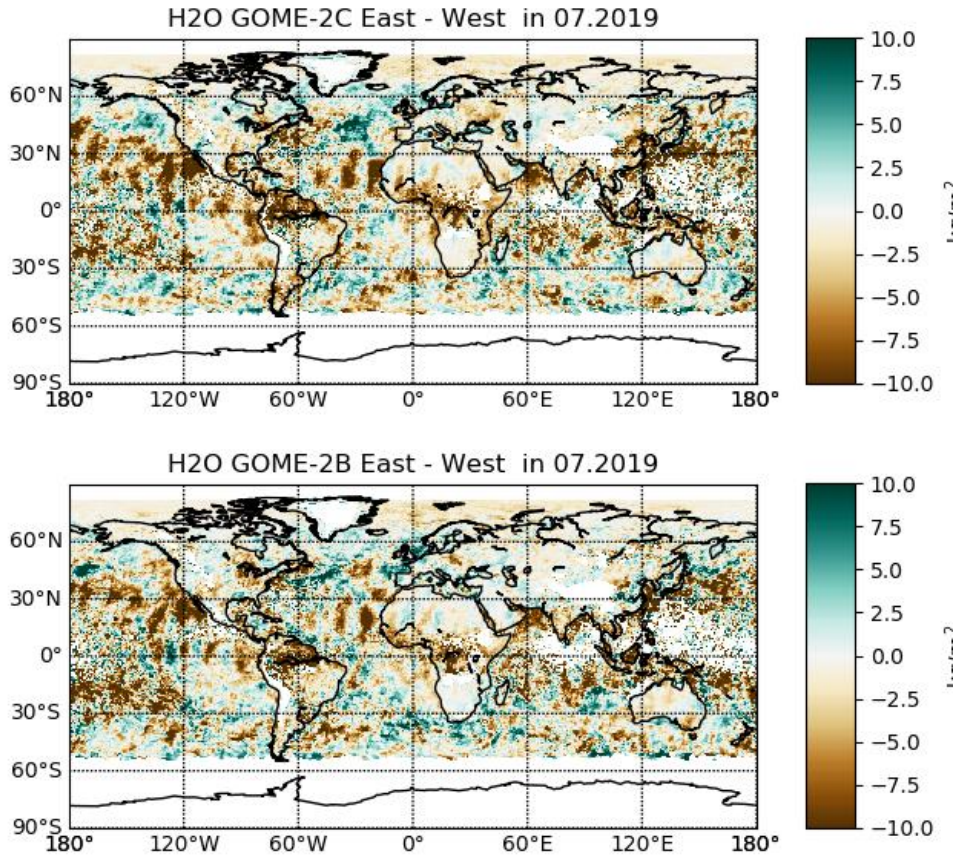


Figure 2-12 As Figure 2-11, but for July 2019

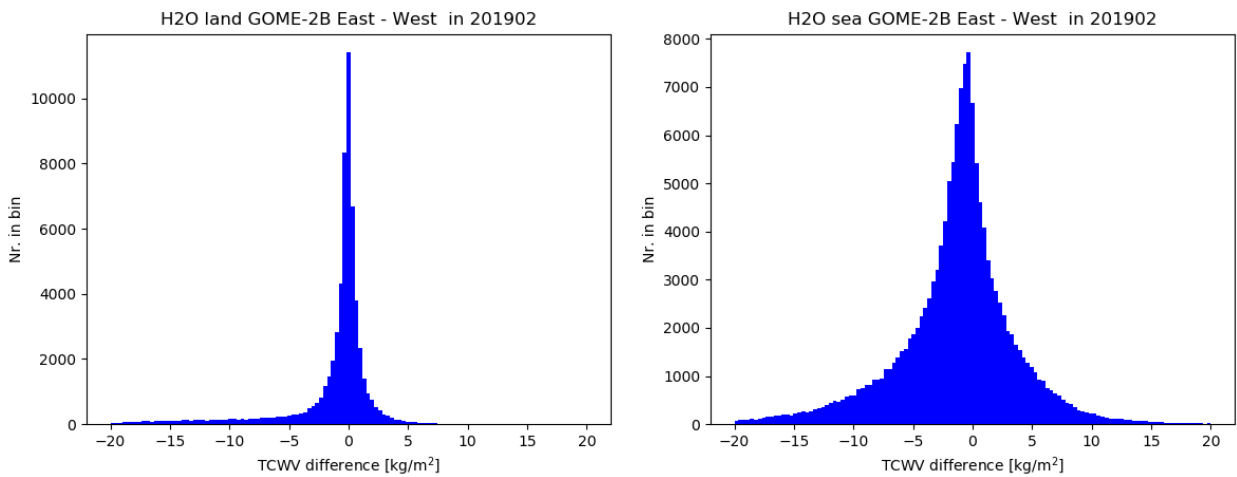


Figure 2-13 Histograms of the East-West difference in TCWV for GOME-2B in Feb.2019: for land surfaces (left panel) and for sea surfaces (right panel)

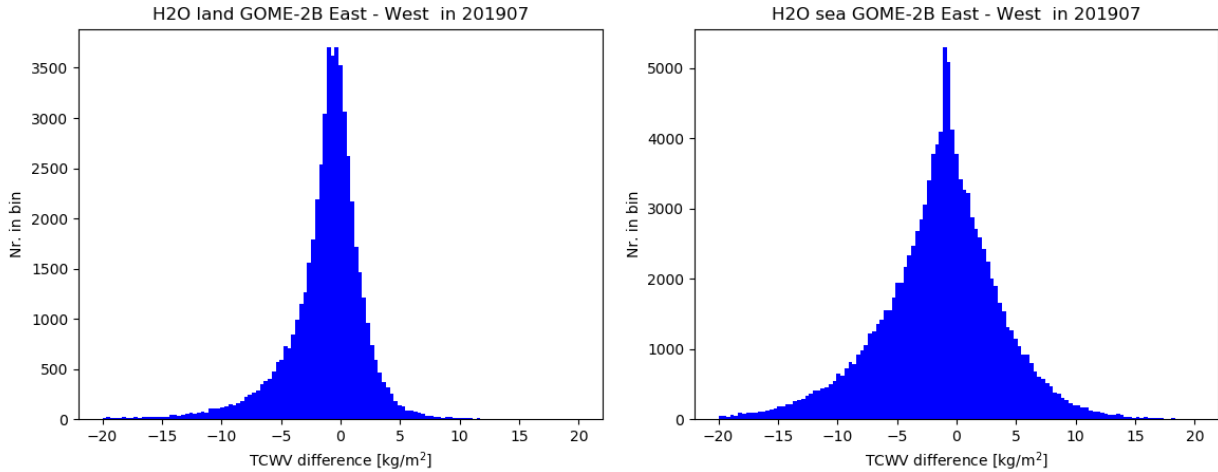


Figure 2-14 As Figure 2-13 but for July 2019

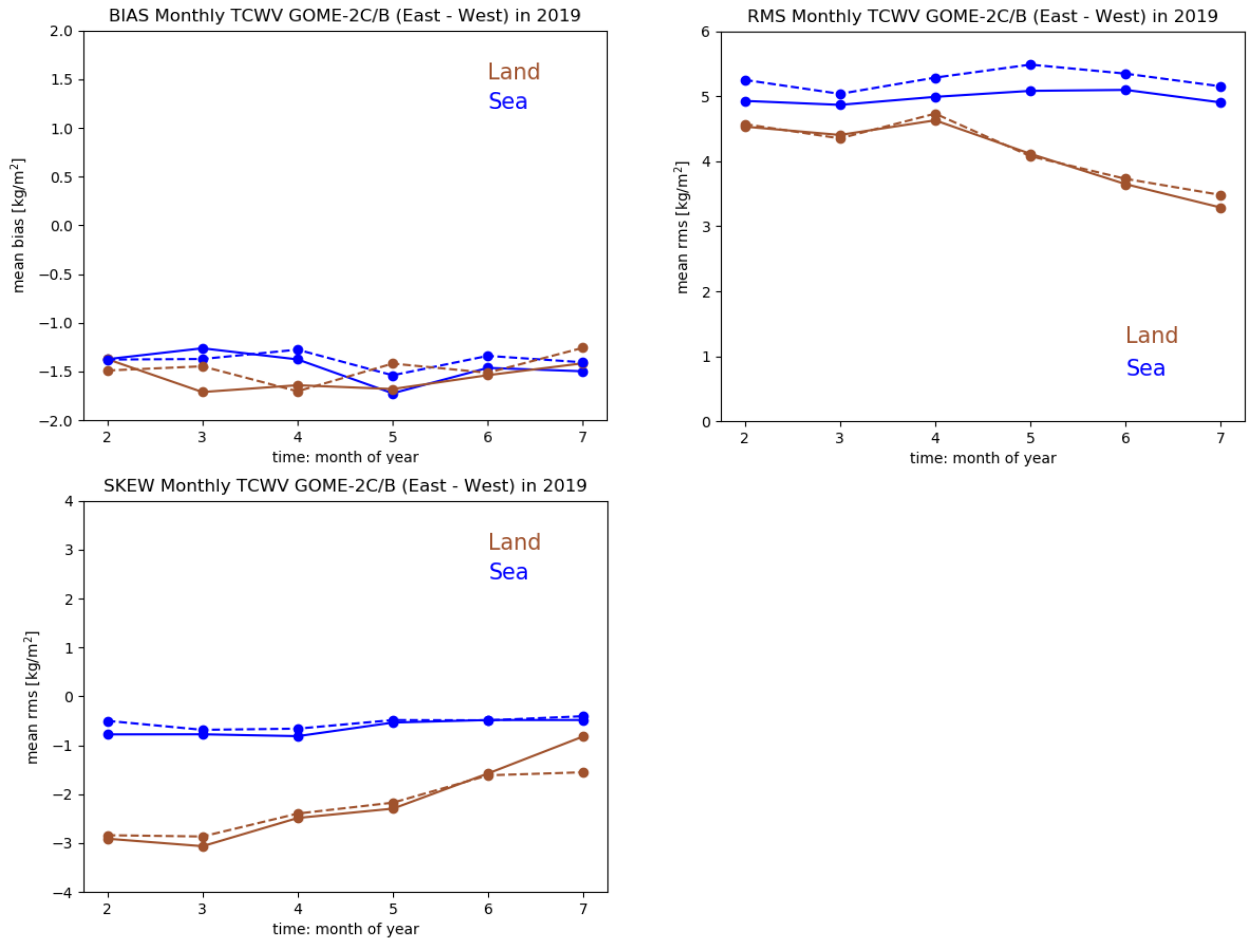


Figure 2-15 Mean bias (left upper panel), RMS (right upper panel) and skew of the distribution of East-West TCWW difference (land brown, sea blue curves) for each month; for GOME-2C (solid line) and GOME-2B (dotted line).

2.4 Discussion and conclusion

TCWV data from GOME-2C have been compared to those of GOME-2B, for the analysis period of February 2019 to July 2019. The quality of the GOME-2C and GOME-2B TCWV data is very similar. Monthly maps, gridded on a resolution of $0.5^\circ \times 0.5^\circ$ latitude/longitude, show a mean wet bias of around 0.5 kg/m^2 for GOME-2C w.r.t. GOME-2B, and a RMS difference of around 2 kg/m^2 . The latter is in line with the retrieval errors quoted in the product. There is no significant difference between land and sea surfaces, although the RMS is a bit larger for sea surface in summer.

A direct comparison of level 2 TCWV products from GOME-2C and GOME-2B, using co-located gridded data, yields a *dry* bias for GOME-2C w.r.t. GOME-2B of -0.6 kg/m^2 in February to -0.2 kg/m^2 in July. The difference with the monthly mean TCWV could be traced down to an East-West effect in the scan lines of the GOME-2 retrievals. Co-located data originate mainly from “West” pixels of GOME-2C, but from “East” pixels of GOME-2B.

For each instrument, the East-West effect looks patchy on a global map. The bias arises mainly from the tail of the distribution of East-West differences. Geographical regions with large positive or negative bias correlate roughly with regions with high standard deviation between daily TCWV measurements and regions with large cloud screening. High standard deviation signifies a high natural variability and was found in earlier validation reports (Grossi et al) to correlate with variability in cloud cover.

Since the East-West effect is very similar for GOME-2C and GOME-2B, it is therefore expected that the East-West bias originates from the treatment of clouds in the algorithm, where the cloud correction algorithm assigns statistically a higher TCWV to West pixels than to East pixels. The latter conclusion is based on the fact that the global East-West bias is very similar for each month, although various regional patches in latitude/longitude may show random East-West behaviour from month to month.

Summarising we conclude that TCWV from GOME-2C is very similar and consistent (within the retrieval uncertainty) with TCWV from GOME-2B.

2.5 Reference documents

Grossi, M., Valks, P., Loyola, D., Aberle, B., Slijkhuis, S., Wagner, T., Beirle, S., and Lang, R.: *Total column water vapour measurements from GOME-2 MetOp-A and MetOp-B*, Atmos. Meas. Tech., 8, 1111-1133, doi:10.5194/amt-8-1111-2015, 2015

Grossi, M., Kalakoski, N., Valks, P.: *O3M SAF Validation Report, Offline Total Water Vapour*, SAF/O3M/DLR/ORR/H2O, 2015

Valks, P., Grossi, M., Slijkhuis, S., Schröder, M., Höschel, H.: *O3M SAF Validation Report, Level-3 Total H2O Data Record from GOME-2A&B*, SAF/AC/DLR/VR/L3_H2O, 2017

Wagner, T., Beirle, S., and Mies, C.: Description of the MPI-Mainz H2O retrieval (Version 5.0, March 2011), technical document, http://www.sciamachy.org/products/H2O/H2Ovc_IUP_AD.pdf

3 Comparison against radiosonde and GPS observations

3.1 Introduction

In this section we show the results of the comparisons of GOME-2C TCWV against water vapour observations based on radiosoundings from Integrated Global Radiosonde Archive (IGRA) and GPS observations from Suominet network.

3.2 Reference observations and co-locations

3.2.1 Integrated Global Radiosonde Archive (IGRA)

Water vapour column data used for comparisons was obtained from the Integrated Global Radiosonde Archive (IGRA). IGRA is a radiosonde dataset maintained by National Climatic Data Center (NCDC). IGRA contains quality-assured observations from 1500 globally distributed stations with different periods of record from 1960s to present. For the period of this validation, the data source is the NCDC real-time Global Telecommunication System (GTS) dataset. Quality assurance procedures are described in detail in Durre et. al (2006). Locations of the IGRA stations with GOME-2C co-locations are shown in figure Figure 3-1.

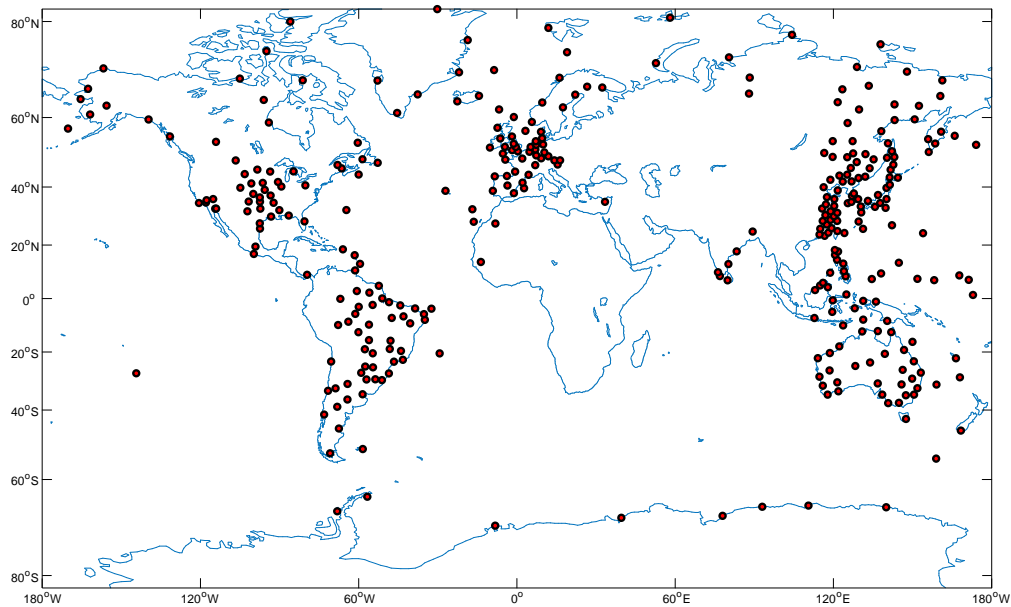


Figure 3-1 Locations of IGRA stations with GOME-2C co-locations.

3.2.2 Suominet

GPS observations were obtained from the COSMIC/SuomiNet network, a ground-based GPS network designed for real-time remote sensing of atmospheric water vapour. The network provides integrated atmospheric water vapour columns and the total electron content from globally distributed GPS stations. However, as of January 2019, only observations from stations located in North America are available. Precipitable water estimates are provided for each station at 30 min time resolution. Locations of the Suominet stations with GOME-2C co-locations are shown in Figure 3-2.

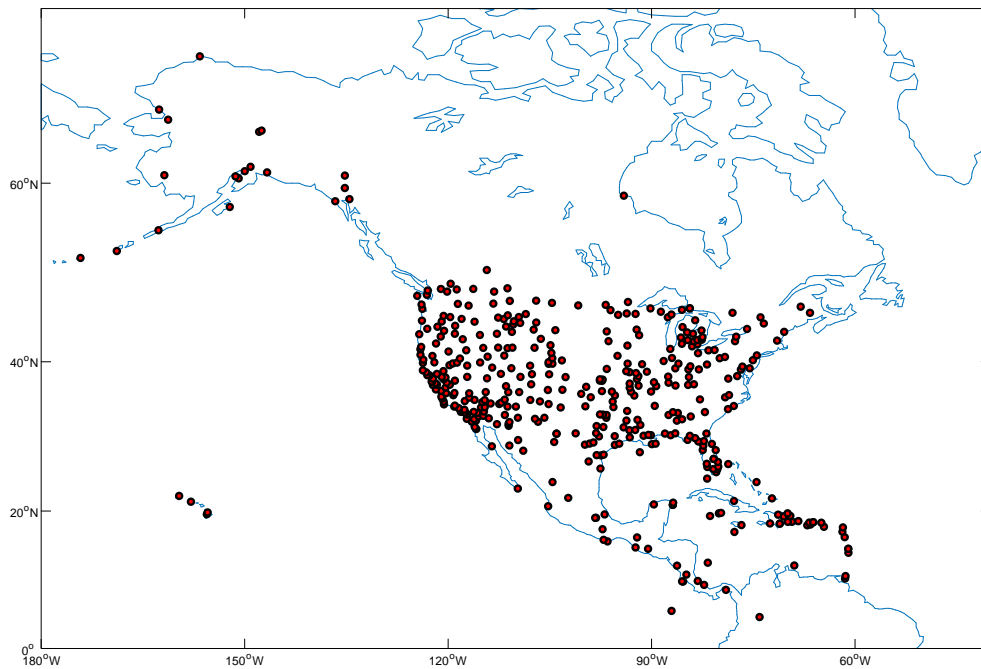


Figure 3-2 Locations of Suominet stations with GOME-2C co-locations.

3.2.3 Co-location criteria

In all comparisons against ground-based observations, the GOME-2C measurements were screened for cloudy scenes using the cloud flag included in the product files. The measurements with solar zenith angle $> 75^\circ$ were discarded to exclude low light conditions. Only forward-scan pixels were used for comparisons, since back-scan pixels are of a larger size. Comparisons with GOME-2C are carried out against both radio-sonde and GPS observations between February and September 2019.

For our analysis of the radiosoundings, we selected the measurements where the stations are located within 0.5 degrees of the center of GOME-2 ground pixel and the sounding times coincide within 90 minutes of the Metop overpass. The water vapour columns were calculated by integrating the specific humidity measurements from the surface up to the altitude of the lapse-rate tropopause, which is specified in the IGRA profiles. Soundings without an identified tropopause were discarded. Only profiles with more than 20 altitude levels were used for the analysis. After the screening, the total number of co-locations with the radiosondes was about 30000.

Similarly, we use GPS measurements located within 0.5 degrees of the center of GOME-2 ground pixel. Because of the better temporal resolution of the GPS measurements, only the observations with smallest available time difference to the MetOp overpass were selected for each coincidence. Since the GPS retrievals are available all day at a frequency of 30 minutes, only co-locations where the time difference between the GOME-2 overpass and the GPS retrieval was less than 15 minutes were used. The total number of co-locations with the GPS was about 72,000.

Locations of the radiosonde and GPS co-locations for GOME-2C are shown in Figure 3-1 and Figure 3-2. While radiosonde observations are widely available, co-location criteria mean that accepted co-

locations are concentrated in two bands (South America to Europe and Western Pacific). Since GPS co-locations are available at smaller time intervals, overpass times do not add further limit to geographical representation. However, Suominet observations are currently only available from American stations.

3.3 Results

General comparisons against IGRA radiosondes and Suominet GPS are shown as scatter plots in Figure 3-3 and Figure 3-4. Statistics of the comparisons are shown in Table 3-1 *Statistical descriptors of comparisons for all co-locations between GOME-2C and IGRA and Suominet observations*. Both comparisons show good general agreement between GOME-2C and reference dataset. Against radiosondes, median bias remains small up to total columns of 50 kg/m². Against GPS observations, bias grows with larger total columns, with dry bias observed above about 20 kg/m². GOME-2C observations are very well correlated with both reference dataset, with correlation coefficients above 0.9 in both cases.

Biases at different levels of total water vapour are also shown in Figure 3-5 and Figure 3-7. In both cases figure shows the median biases as well as 5th, 25th, 75th and 95th percentiles of the difference, binned at 1 kg/m² intervals. In top rows the binning is against GOME-2C total column and in the bottom row, against the radiosonde (Figure 3-5) or GPS (Figure 3-7). This comparison illustrates some aspects of the scatterplots. In radiosonde comparisons, GOME-2C total columns below 40 kg/m² agree very well with soundings, while above that GOME-2C shows a growing wet bias, reaching about 20 % at 60 kg/m². In contrast, when binned against radiosoundings, agreement stays good until above 50 kg/m², with GOME-2C showing dry bias when very high total columns are observed with radiosonde. In similar comparisons against GPS observations, GOME-2C shows a growing dry bias with both comparisons. However, similar to radiosonde comparisons, for GOME-2C columns above 40 kg/m², this strong wet bias is again seen.

Figure 3-6 and Figure 3-8 show the dependence of the error on Solar zenith angle, cloud fraction, and surface albedo. Bias against radiosoundings does not depend strongly on the SZA of the observation, while the median difference against GPS observations changes from negative to positive around 50° SZA. Above that, relative difference shows strong positive bias, peaking at 44 % at 72° SZA. It should be noted, that for observations at high SZAs, total columns are generally very low leading to high relative differences.

Cloud fraction affects the bias in a similar way in both comparisons. For cloud fractions below 0.2 (clear-sky) biases are generally more positive (wet) than for higher cloud fractions. This is especially noticeable in comparisons against the GPS observations, where the dry bias in Figure 3-4 can be largely attributed to the difference of the effect of cloud cover on the observations.

Effect of the surface albedo on the difference is small, except for very dark surfaces, where a wet bias is observed. Based on previous work, the wet bias over the darkest surfaces is mainly due to wet bias over ocean pixels, that dominate the lowest bin of the comparison.

In conclusion, the GOME-2C Total Water Vapour column generally agrees well with both IGRA radiosondes and Suominet GPS observations.

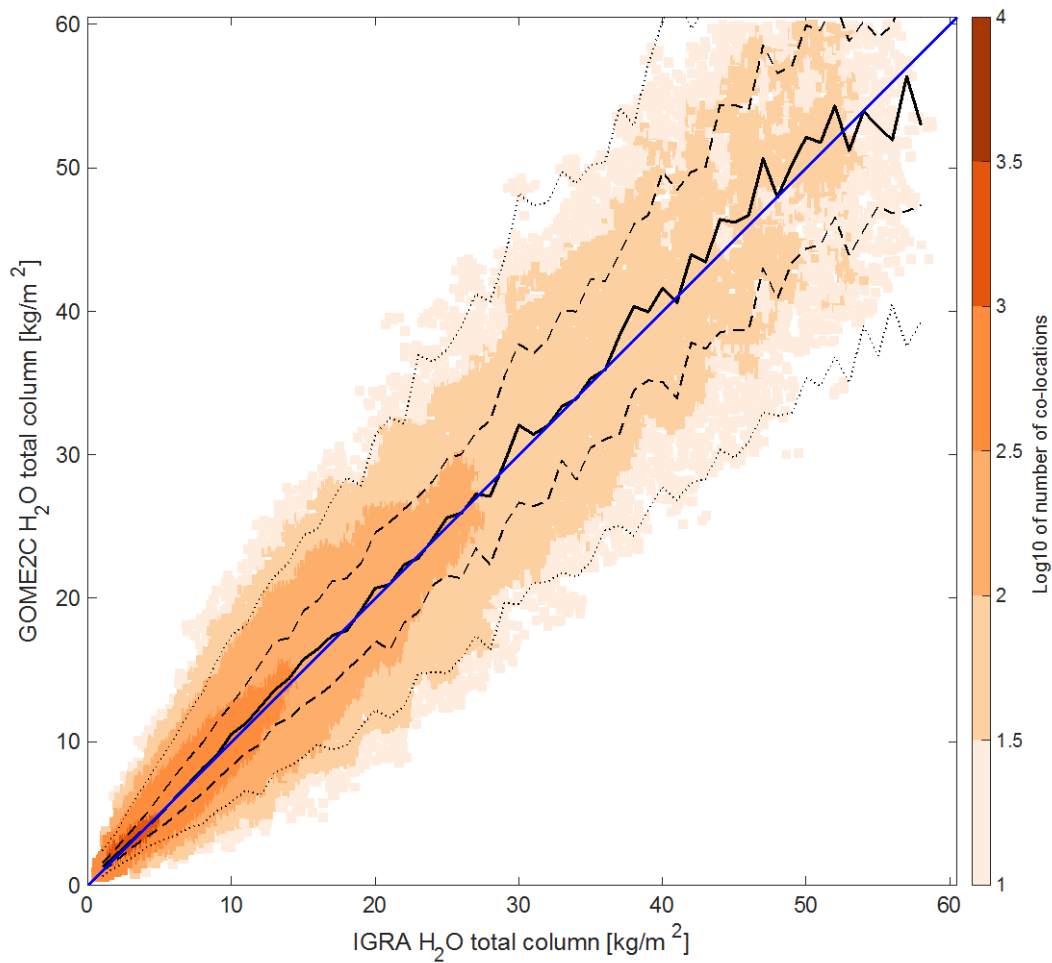


Figure 3-3 Scatterplot of GOME-2C co-locations between GOME-2C and IGRA radiosoundings. Color represents the number of co-locations in each 1x1 kg/m² grid point. Black lines show the median (solid line), 25 %, 75 % (dashed lines), 5 % and 95 % (dotted lines) percentiles of the distribution, binned according to IGRA total columns at 1 kg/m² intervals. Blue line shows the x=y line.

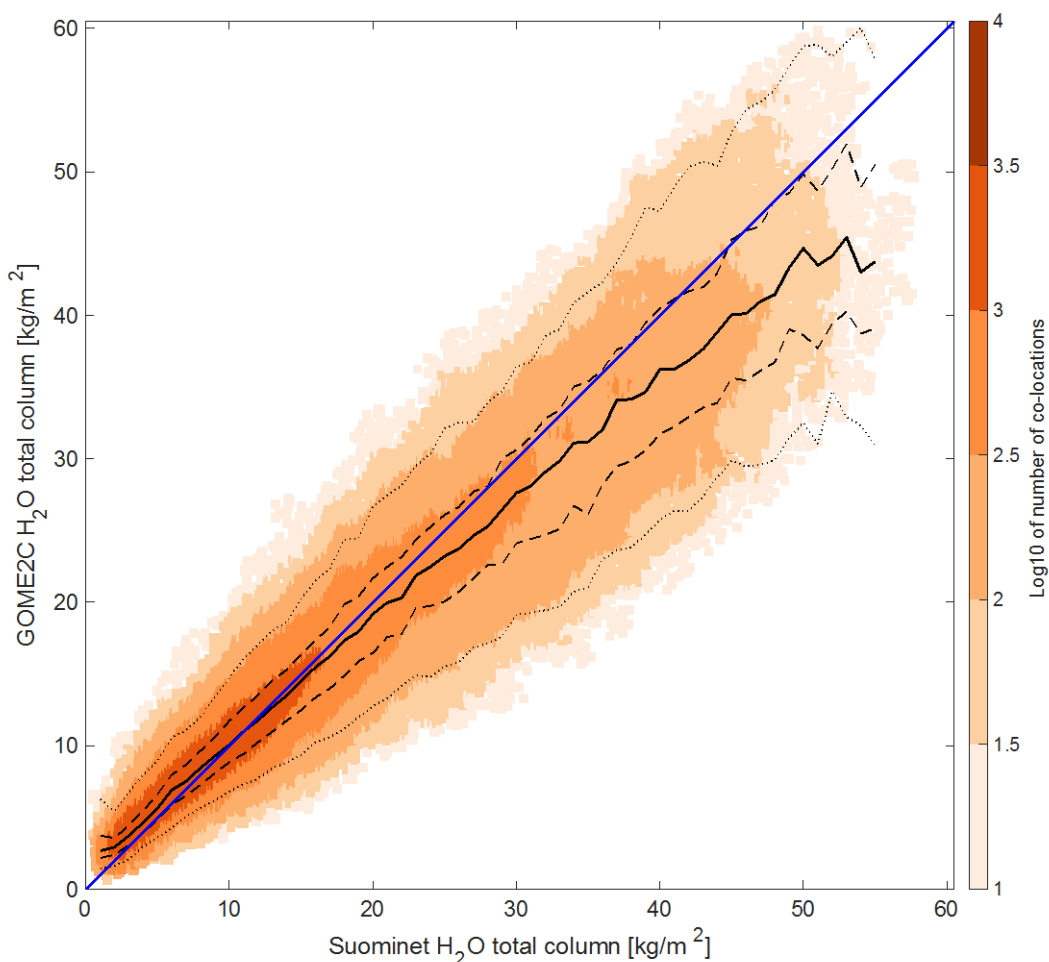


Figure 3-4 Scatterplot of GOME-2C co-locations between GOME-2C and Suominet GPS observations. Color represents the number of co-locations in each 1x1 kg/m² grid point. Black lines show the median (solid line), 25 %, 75 % (dashed lines), 5 % and 95 % (dotted lines) percentiles of the distribution, binned according to Suominet total columns at 1 kg/m² intervals. Blue line shows the x=y line.

Table 3-1 Statistical descriptors of comparisons for all co-locations between GOME-2C and IGRA and Suominet observations.

	IGRA	Suominet
N	30128	72087
Correlation coefficient	0.920	0.915
Mean difference [kg/m ²]	0.751	-1.316
Mean relative difference [%]	5.1	0.8
Standard Deviation [kg/m ²]	6.53	5.14
Median difference [kg/m ²]	0.171	-0.503
Median relative difference [%]	1.8	-3.3

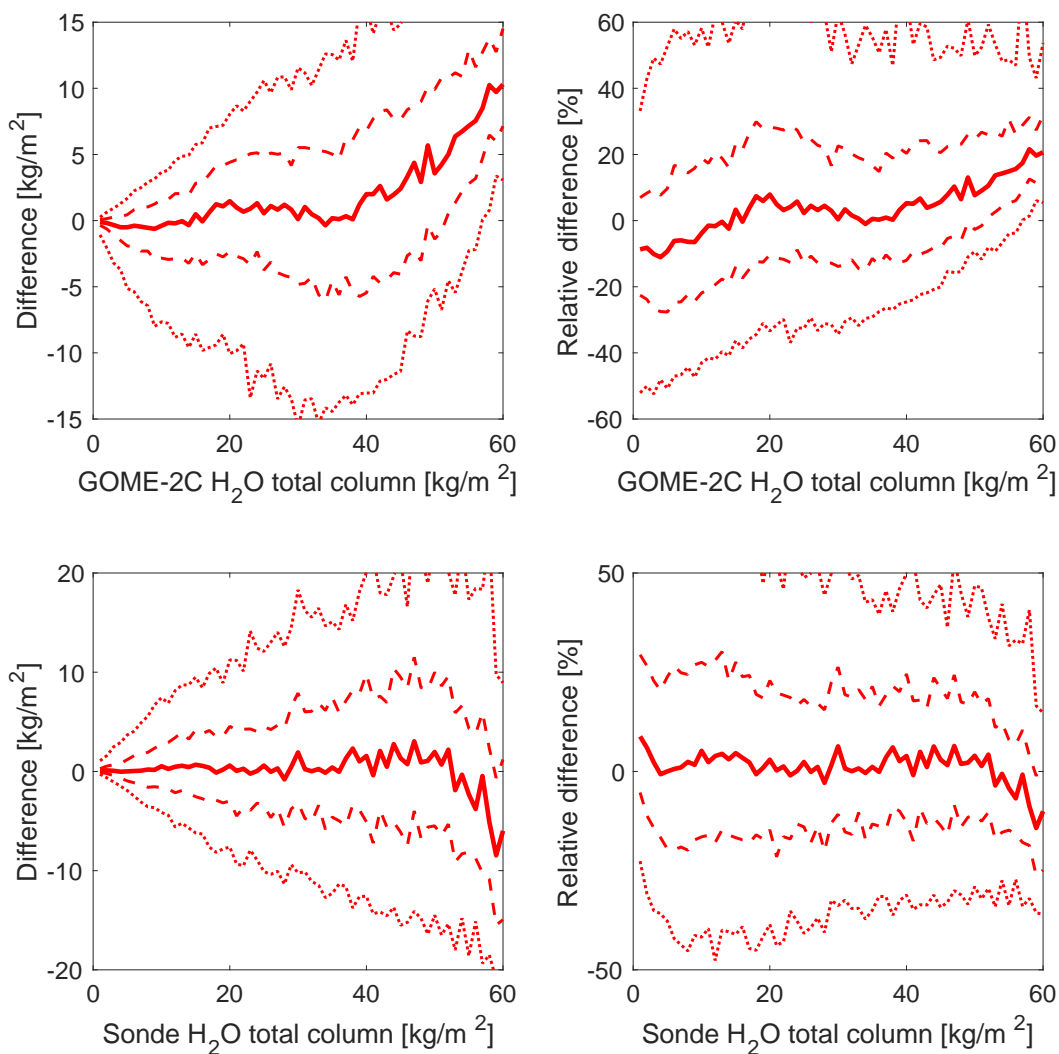


Figure 3-5 Difference GOME-2C - IGRA as a function of GOME-2C (top) and IGRA (bottom) TWV. Left panels show the difference in kg/m², right in %. Solid lines show the median value, dashed lines 25th and 75th percentiles and dotted lines 5th and 95th percentiles.

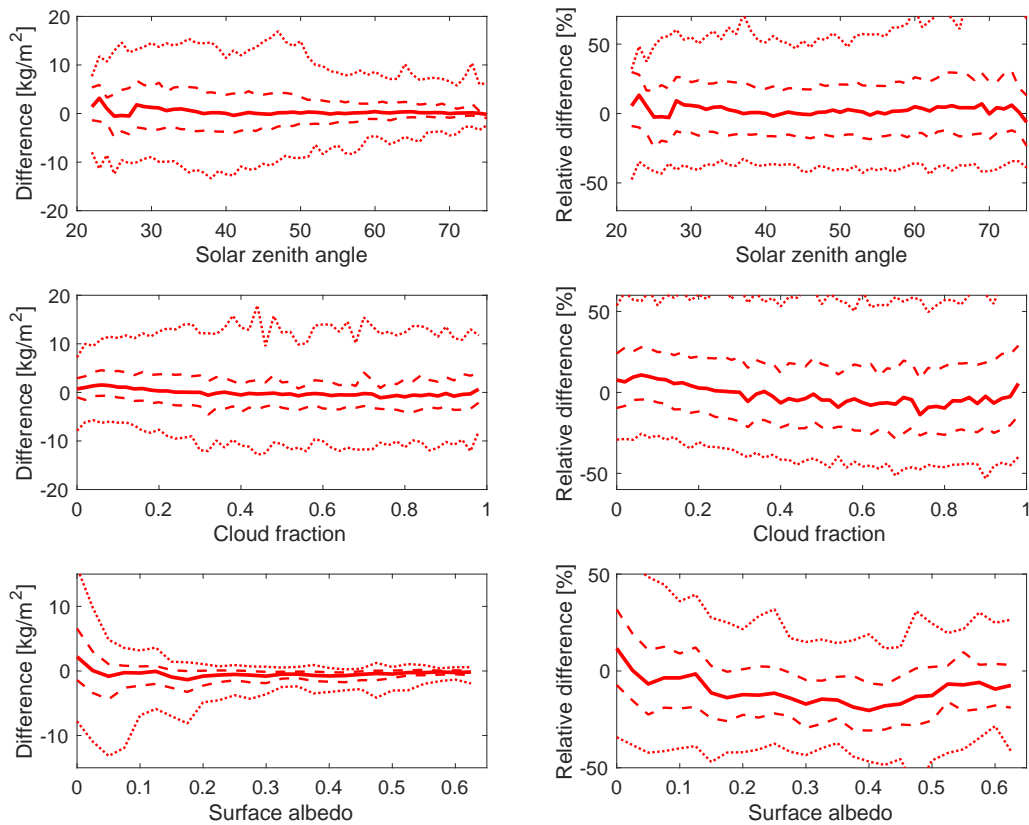


Figure 3-6 Difference GOME-2C - IGRA as a function of Solar zenith angle (top), cloud fraction (middle) and surface albedo (bottom) TWV. Left panels show the difference in kg/m², right in %. Solid lines show the median value, dashed lines 25th and 75th percentiles and dotted lines 5th and 95th percentiles.

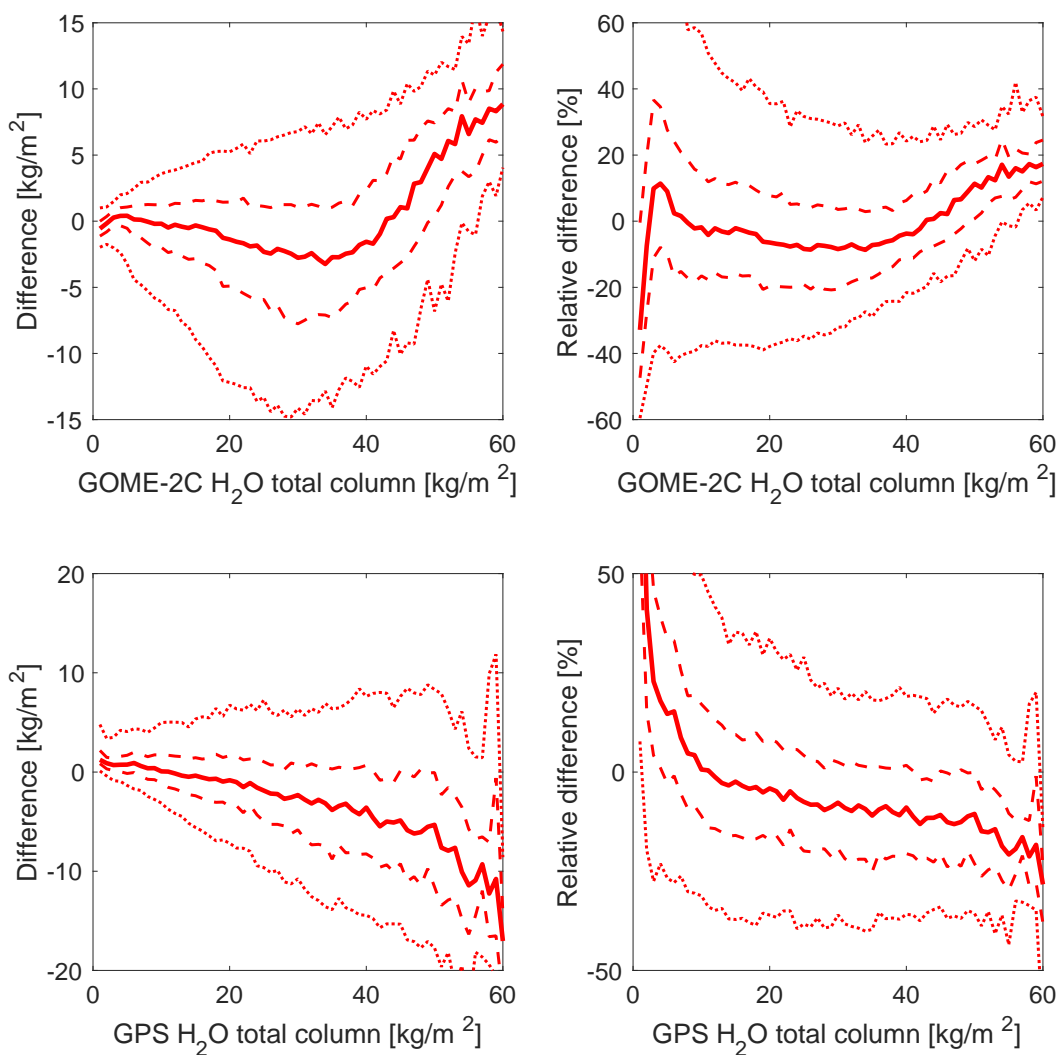


Figure 3-7 Difference GOME-2C - Suominet as a function of GOME-2C (top) and Suominet (bottom) TWV. Left panels show the difference in kg/m², right in %. Solid lines show the median value, dashed lines 25th and 75th percentiles and dotted lines 5th and 95th percentiles.

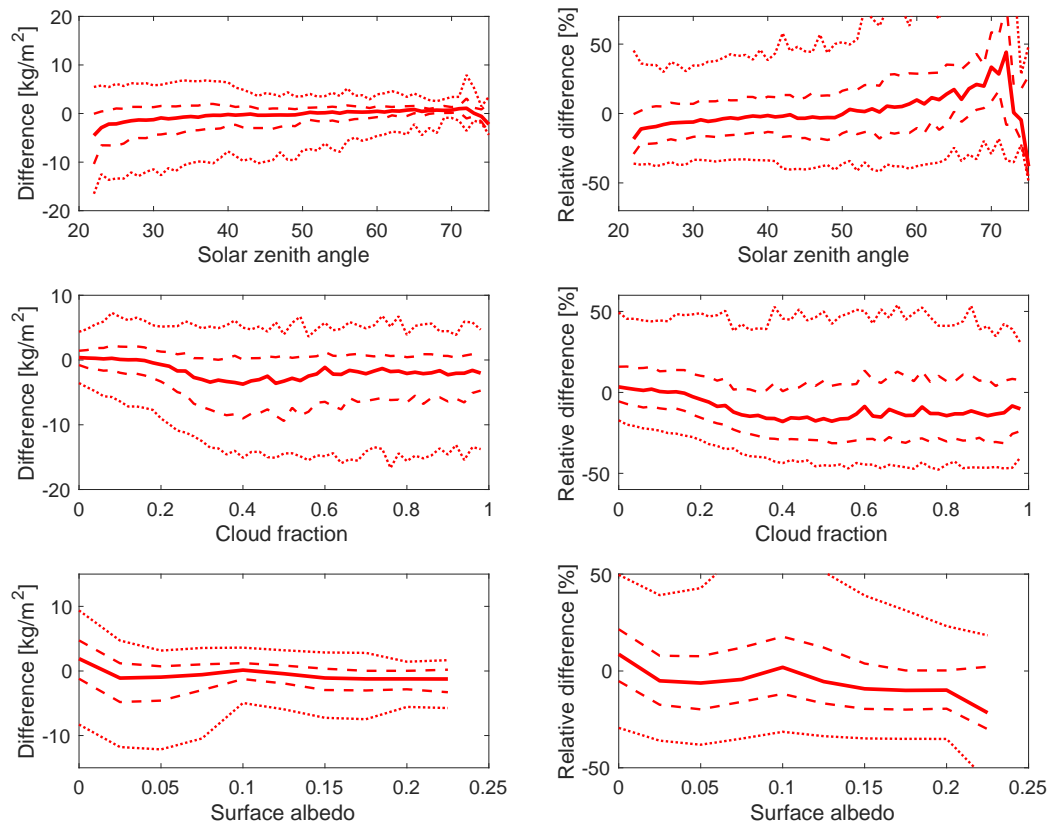


Figure 3-8 Difference GOME-2C - Suominet as a function of Solar zenith angle (top), cloud fraction (middle) and surface albedo (bottom) TWC. Left panels show the difference in kg/m², right in %. Solid lines show the median value, dashed lines 25th and 75th percentiles and dotted lines 5th and 95th percentiles.

3.4 Reference Documents

Kalakovski, N., Kujanpää, J., Sofieva, V., Tamminen, J., Grossi, M., and Valks, P.: Validation of GOME-2/Metop total column water vapour with ground-based and in situ measurements, *Atmos. Meas. Tech.*, 9, 1533-1544, <https://doi.org/10.5194/amt-9-1533-2016>, 2016.

Grossi, M., Kalakovski, N., Valks, P.: *O3M SAF Validation Report, Offline Total Water Vapour*, SAF/O3M/DLR/ORR/H2O, 2015